Article

Differential Fluorescent Chemosensing of Antibiotics Using a Luminescent Zn(II) Coordination Polymer Based on a 4-Amino-1,8-naphthalimide Tröger's Base Fluorophore

Purti Patel [†]**, Mannanthara Kunhumon Noushija** [†] **and Sankarasekaran Shanmugaraju** *

Department of Chemistry, Indian Institute of Technology Palakkad, Palakkad 678557, Kerala, India; 202105007@smail.iitpkd.ac.in (P.P.); 202114001@smail.iitpkd.ac.in (M.K.N.)

* Correspondence: shanmugam@iitpkd.ac.in
† These authors contributed equally to this work.

Abstract: The design and development of useful chemosensors for the ultra-trace detection of environmental pollutants and contaminants is a topical area of research. Herein, we report a new nanoscale emissive Zn(II) coordination polymer (**TB-Zn-CP**) for differential fluorescence sensing of various antibiotics in water. **TB-Zn-CP** was synthesized using a unique V-shaped green emitting 4-amino-1,8-naphthalimide Tröger's base (**TBNap**) fluorophore. The structural and morphological features of **TB-Zn-CP** were characterized by various standard spectroscopic and microscopy techniques. The fluorescence titration studies in water demonstrated a remarkable sensitivity and differential fluorescence sensing properties of **TB-Zn-CP** for the fast detection of different antibiotics. Among different antibiotics, chloramphenicol (CRP), 1,2-dimethyl-5-nitroimidazole (DMZ), and sulfamethazine (SMZ) displayed the highest fluorescence-quenching efficiency and superior sensitivity in their detection. The differential sensing capability of **TB-Zn-CP** was also indicated by visualizable color changes. The Stern–Volmer quenching constant K_{SV} was determined to be in the order of 10^3–10^4 M^{-1}, and the sensitivity was shown to be at a nanomolar (10^{-9} M) level. All these results confirm that **TB-Zn-CP** can be a potential and practically useful polymeric sensor for differential fluorescence and visual detection of different antibiotics in water.

Keywords: 4-amino-1,8-naphthalimide; Tröger's bases; Zn(II) coordination polymer; infinite coordination polymer particles; fluorescence sensors; antibiotics

1. Introduction

Since the 1940s, various bacterial infections and illnesses have been treated by different antibiotics [1]. Today, antibiotics have become a cornerstone in treating various infections in humans as well as in animals, experiencing widespread use in healthcare and animal farming industries [2,3]. Additionally, in the natural environment, antibiotics serve as vital tools for the survival and competitive advantage of organisms, often referred to as the weapons of producer microorganisms [4]. These microorganisms employ antibiotics to compete with other microbes, eliminating rival bacteria and establishing dominance in the microbial community [5]. However, the extensive use of antibiotics by living systems has led to their large accumulation in water streams and ecosystems [6]. The environmental contamination due to antibiotics stems from their excessive consumption, improper excretion practices, and inadequate disposal methods, posing risks to human health and environmental well-being [7]. Even though they are important in both animal and human life, the indiscriminate and excessive use of antibiotics considerably contributes to the emergence of resistant strains [1]. According to the World Health Organization (WHO), "antibiotic resistance" poses a severe economic and sociological risk to public health [2,3]. Due to their lengthy persistence in the natural environment and the harm that they do to living things, several antibiotics have been identified as potential environmental pollutants,

including penicillin, fluoroquinolones, lactams, tetracyclines, and so on [8]. For instance, continuous intake of antibiotics can weaken immunity and lead to hepatotoxicity, allergic reactions, gastrointestinal disturbances, genetic problems, and various diseases [9,10]. Over the next 35 years, 300 million premature deaths are predicted worldwide if the current trend holds [11,12]. Therefore, addressing the overuse and inappropriate disposal of antibiotics is crucial to mitigating the growing threats of antibiotic resistance and safeguarding both human health and the environment. Dose modification and trace-level antibiotic monitoring are highly recommended to reduce the prevalence of antibiotic-resistant bacteria [13]. For the well-being of human health and to protect the environment, it is essential to find an efficient and feasible detection method with high selectivity for the sensitive analysis and identification of antibiotics.

Several analytical techniques have been used so far for precise and trustworthy monitoring of antibiotic residues in natural resources, including liquid chromatography–mass spectrometry (LC-MS), high-performance liquid chromatography (HPLC), electro-kinetic capillary chromatography (EC), and surface-enhanced Raman spectroscopy (SERS) [14–17]. All of these techniques, meanwhile, are time-consuming and expensive and call for sophisticated machinery and skilled labor [16,17]. Additionally, despite the development of numerous techniques, including photolysis, hydrolysis, thermolysis, technical oxidation processes, and biodegradation, all of which are based on chemical treatment, technologies for the efficient detection and removal of antibiotics are still in their infancy. In recent years, researchers have been very concerned with developing portable, trustworthy, and affordable methodologies and technologies for selective sensing and determining antibiotic contaminant concentrations in water bodies [18–20]. Luminescence-based detection and surface adsorption methods are promising for antibiotic sensing and removal due to their simplicity, high sensitivity, and enhanced adsorption efficiency [21,22]. However, the challenge lies in finding a suitable material that can exhibit highly selective and superior sensitivity for the detection of particular types of antibiotics [23–25]. Coordination polymers (CPs), an emerging class of organic–inorganic hybrid materials, are regarded as an advantageous platform for detection, sensing [26,27], and adsorption [28,29] applications due to their unique electronic and optical properties, high surface area, easily adaptable structures, and functions.

On the other hand, fluorescence-based sensing is known for its high sensitivity and straightforward visualization and has become a promising and cost-effective sensing method for the detection of environmental pollutants [30–34]. In light of this, in the past years, luminescent CPs have gained special research attention for their potential in detecting antibiotics [35–42]. The fluorescence properties and sensing capabilities of CPs can be easily tailored by selecting and combining pre-designed multidentate organic linkers and metal ions, or by incorporating suitable fluorescent signal molecules [43–46]. Reducing the particle size of bulk crystalline coordination polymers (CPs) to the micro- and nanoscale is demonstrated to enhance their solution processibility in aqueous environments, elevate their interaction with analytes, and improve their sensing capacity [47]. However, only a limited number of luminous nanoscale coordination polymers have been developed to date and utilized as potential fluorescence sensors for antibiotic detection. To enhance the selectivity of CPs in detecting antibiotics, a proposed method involves incorporating Lewis base functional groups, such as amines and pyridines. These groups can potentially detect antibiotics through intermolecular H-bonding interactions with the hydrogen bond donor groups like hydroxy and amine groups of antibiotics [23,48–52].

Considering these aspects, herein, we designed and synthesized a new fluorescent nanoscale Zn(II) coordination polymer, **TB-Zn-CP,** built from a green-emitting 3-picolyl-4-amino-1,8-naphthalimide Tröger's base (**TBNap**) fluorophore [53–57]. The intrinsic chirality of Tröger's base moiety favors the unusual V-shaped configuration of two 4-amino-1,8-naphthalimides, which facilitates the guest binding through numerous supramolecular interactions and demonstrates the enhanced sensing capability for analyte detection. We foresaw that Tröger's base's Lewis base properties would boost the selectivity of **TB-Zn-CP** for the differential detection of antibiotics via intermolecular hydrogen-bonding interac-

tions [58]. Indeed, **TB-Zn-CP** has demonstrated remarkable sensitivity and differential sensing capabilities for the rapid detection of antibiotics in an aqueous medium. Fluorescent titration studies have revealed that **TB-Zn-CP** exhibits preferential binding of Chloramphenicol (CRP), 1,2-Dimethyl-5-nitroimidazole (DMZ), and Sulfamethazine (SMZ) antibiotics, displaying superior sensitivity in their detection. Notably, other antibiotics have shown minimal to moderate binding affinity and, thus, fluorescence emission quenching. The differential fluorescence-sensing ability of **TB-Zn-CP** towards different antibiotics was also seen by sharp color changes before and after the mixing of antibiotics in water.

2. Experimental

2.1. Materials

All reagents, solvents, and starting precursors were procured from Sigma-Aldrich (Bangalore, India) and utilized without further purification. For the synthesis of **TB-Nap** and **TB-Zn-CP**, commercially available reagent-grade chemicals were employed. Spectroscopy-grade solvents from Merck were used without additional purification. 4-nitro-1,8-naphthalic anhydride, 3-picolylamine, palladium on carbon (10 wt.% loadings), paraformaldehyde, and trifluoroacetic acid (TFA) were sourced from Sigma-Aldrich and used in their as-received state. Reagent-grade antibiotics analytes, essential for sensing studies, were obtained from the Tokyo Chemical Industry (Hyderabad, India) and used as purchased. Deuterated solvent $(CD_3)_2SO$, employed for NMR analyses of the monomer, was acquired from Sigma-Aldrich. The synthesis of organic linker **TBNap** followed the procedure outlined in the literature [59].

2.2. Instrumentations

The as-synthesized **TB-Zn-CP** was dried under a high vacuum to remove the trapped solvents before its characterization. The FT-IR spectrums of polymer **TB-Zn-CP** and ligand **TBNap** were obtained using the Shimadzu Scientific Instruments (IR Tracer 100) (Science Park, Singapore, Singapore) equipped with an ATR sampler. Thermogravimetric analysis (TGA) of **TB-Zn-CP** was conducted on the PerkinElmer STA 8000 analyzer (Thane, India), which featured an ultra-microbalance with a sensitivity of 0.1 mg. The analysis spanned a temperature range from 30 °C to 1000 °C, with a scan rate of 10 °C min^{-1} under N_2 purge. Powder X-ray diffraction analysis of **TB-Zn-CP** and **TBNap** was carried out on a Rigaku (XRD Smart Lab) diffractometer operating at 9 kW (Bangalore, India). Dynamic Light Scattering (DLS) analysis of **TB-Zn-CP** was carried out using Malvern Panalytical Zetasizer (Bangalore, India) at PSG Institute of Advanced Studies, Coimbatore. The particle size analysis was performed by keeping the sample temperature at 25 °C. The surface morphology of **TB-Zn-CP** was visualized using field emission scanning electron microscopy (FE-SEM) on a Carl Zeiss (Gemini SEM 300) microscope. Sample preparation involved drop-casting the aqueous suspension of the as-synthesized polymer onto a stub, followed by coating with Au and drying under vacuum before imaging. The UV–visible absorption titration studies were carried out using a Thermo Fisher scientific absorption spectrometer in a 1 cm quartz cuvette, with baseline correction applied to all measurements (Waltham, MA, USA). The fluorescence titration studies were performed on a PerkinElmer FL-8500 fluorescence spectrophotometer (Waltham, MA, USA), which featured a Xenon arc (150 W) light source. The measurements were conducted at a constant temperature of 298 K, utilizing a quartz cuvette and a scan rate of 1200 nm min^{-1}. The results obtained were graphically represented using Origin Pro 8.5 software.

2.3. Synthesis and Characterization of Coordination Polymer TB-Zn-CP

The organic linker **TBNap** (10 mg, 0.016 mmol, 1.0 eq.) was taken in a glass vial along with 2 mL of water and then sonication to achieve a well-dispersed suspension. Subsequently, an aqueous solution of $Zn(OAc)_2 \cdot 2H_2O$ (3.5 mg, 0.016 mmol, 1.0 eq.) was added dropwise under constant stirring. After a few minutes of stirring at room temperature, the reaction mixture turned turbid. The reaction mixture was further stirred overnight at 80 °C.

After cooling to room temperature, the reaction mixture was centrifuged, and the resulting precipitate was washed with water (2 × 10 mL) and then dried in an oven for 1 h to isolate the targeted product coordination polymer **TB-Zn-CP** as a yellow powder in 50% yield (calculated based on the organic linker's molecular weight). The formation of **TB-Zn-CP** was fully characterized by using various spectroscopy and microscopy techniques.

2.4. Fluorescence Sensing Studies

To prepare the stock solution, 2 mg of **TB-Zn-CP** was dispersed in 10 mL of deionized water. The resulting suspension was sonicated for 30 min and then allowed to age for one day to form a uniformly dispersed colloidal suspension. Similarly, 1 mM stock solutions of different antibiotics of each were freshly prepared in water. A 50 μL aliquot of the **TB-Zn-CP** colloidal suspension was taken with 1950 μL of water in a 3 mL cuvette for the fluorescence sensing studies. Subsequently, 1 mM stock solutions of individual antibiotics (20 μL at once) were incrementally added to the cuvette containing **TB-Zn-CP** colloidal suspension. The fluorescence emission intensity of **TB-Zn-CP** before and after the addition of antibiotics was measured. For all the fluorescence titration experiments, the sample was excited at λ = 300 nm, and emission was monitored in the range of λ = 550 to 650 nm at 298 K. For all the measurements, the slit width was kept at 10 nm.

The percentage of fluorescence-quenching efficiency of **TB-Zn-CP** towards antibiotics was determined using the following equation:

$$\text{Quenching efficiency (\%)} = (I_0 - I)/I_0 \times 100 \tag{1}$$

where I_0 is the initial fluorescence emission intensity of **TB-Zn-CP** in water, and I is the fluorescence emission intensity after the addition of antibiotic solutions.

The relative changes (I_0/I) in fluorescence emission intensity of **TB-Zn-CP** colloidal suspension with increasing the concentration [Q] of antibiotics was demonstrated by the following the Stern–Volmer equation:

$$(I_0/I) = 1 + K_{SV}[Q] \tag{2}$$

The Stern–Volmer quenching constant (K_{SV}) was determined from the slope of the linear plot of I_0/I vs. Q.

The limit of detection (LoD) was calculated from the fluorescence titration profile using the following equation:
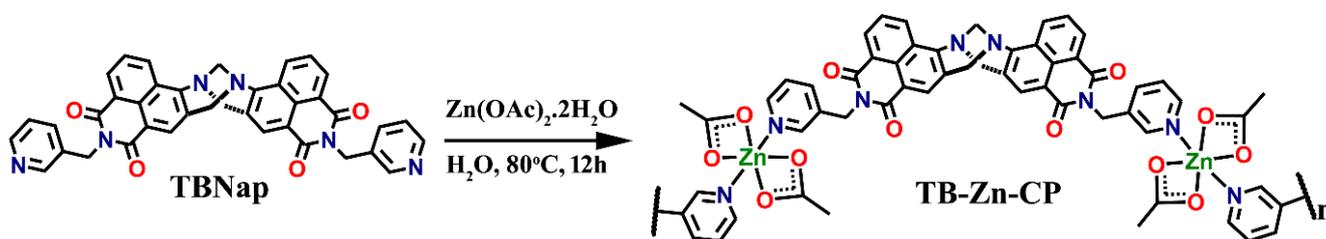
$$\text{Detection limit} = 3\sigma/K \tag{3}$$

where σ is the standard deviation of the initial fluorescence emission intensity in the absence of the antibiotic analytes, and K is the slope of the linear calibration curve.

3. Results and Discussion

3.1. Synthesis and Characterization of TB-Zn-CP

The organic linker **TBNap** was freshly synthesized following the procedure reported in the literature [59]. The commercially purchased precursor, 4-nitro-1,8-naphthalic anhydride, was condensed with 3-picolylamine to isolate *N*-(3-picolyl)-4-nitro-1,8-naphthalimide, which was subsequently reduced to its corresponding amine derivative. *N*-(3-picolyl)-4-amino-1,8-naphthalimide was then reacted with paraformaldehyde in the presence of trifluoroacetic acid to yield **TBNap** in quantitative yield. As shown in Scheme 1, the Zn(II) coordination polymer **TB-Zn-CP** was obtained by stirring Zn(OAc)$_2$·2H$_2$O (1.0 eq.) and the organic ligand **TBNap** (1.0 eq.) in H$_2$O (4 mL) at 80 °C for 12 h. The well-dispersed **TBNap** aqueous suspension was changed to a yellow colloidal suspension after the addition of Zn(OAc)$_2$·2H$_2$O, which evidences the formation of the infinite coordination polymer. The heavy precipitate that formed after cooling to room temperature was collected through centrifugation, and the precipitate was washed with H$_2$O to isolate the coordination

polymer **TB-Zn-CP** as a yellow powder in 50% yield. **TB-Zn-CP** was characterized by using various standard spectroscopy and microscopy techniques.

Scheme 1. Schematic representation of the synthesis of Zn(II) coordination polymer **TB-Zn-CP** from **TBNap**.

As shown in Figure 1A, the FTIR spectrum of **TB-Zn-CP** showed two sharp peaks at 1596 cm^{-1} (for symmetrical) and 1403 cm^{-1} (for asymmetrical), corresponding to the coordinated acetate (-CH$_3$COO-) anions; these peaks were absent in the FTIR spectrum of **TBNap** (see Figure S1, Supplementary Materials). Two sharp bands in the range of 1705 to 1697 cm^{-1} were assigned to the carbonyl (-C=O-) stretching frequencies, and a strong band appeared at 462 cm^{-1}, which was ascribed to the Zn−N coordination bond. The appearance of an intense band at 1074 cm^{-1} confirmed the presence of Tröger's base unit in the isolated solid material. The X-ray powder diffraction analysis of **TB-Zn-CP** showed relatively broader peaks, indicating that the isolated coordination polymer is microcrystalline (Figure 1B). The particle size of the well-dispersed colloidal suspension of **TB-Zn-CP** was measured by Dynamic Light Scattering (DLS) analysis. The average particle size of **TB-Zn-CP** in an aqueous medium is ~81 nm, confirming that **TB-Zn-CP** is a nanoscale polymeric material (see Figure S2, Supplementary Materials). Under a nitrogen atmosphere, the thermal gravimetric analysis (TGA) of **TB-Zn-CP** demonstrated thermal stability up to 400 °C, with approximately 20% of its initial mass retained at 700 °C. Notably, a marginal weight gain (~7%) was observed in the initial phase, likely due to the adsorption of N$_2$ gas within the pores of the coordination polymer (Figure S3, Supplementary Materials). To determine the morphological feature, scanning electron microscopy (SEM) was employed, which revealed a nano-porous sponge-like morphology, as depicted in Figure 1C. Furthermore, the energy-dispersive X-ray spectroscopy (EDX) confirmed the presence of Zn, C, O, and N through distinctive peaks (Figure S4A, Supplementary Materials). Additionally, Quanta mapping highlighted a uniform distribution of Zn, C, O, and N across the entire sample of **TB-Zn-CP** (Figure S4B, Supplementary Materials).

3.2. Fluorescence Sensing of Antibiotics

Amino-1,8-naphthalimide derivatives (**Naps**) are well-known classical fluorophores that are strongly colored and absorbed, and which emit in the visible region of the spectrum. **Naps** are highly emissive due to the excited state internal charge transfer (ICT) transition from the electron-rich amino group to the electron-deficient imide unit [53–55]. On the other hand, Tröger's base is a unique V-shaped and C_2-symmetric organic scaffold with a large internal hydrophobic cavity that can be exploited for host–guest chemistry [56,57]. Given this, over the past several years, we have developed a plethora of amino-1,8-naphthalimide Tröger's bases (**TBNaps**) and employed them as a bifunctional organic scaffold for the development of multifaceted structures, functional materials, and porous organic polymers for their application in environmental-related studies and biomedicine [46,59]. Coordination polymers based on electronically inert Zn(II) metal ions and fluorescence organic linkers are shown to display ligand-based strong photoluminescence properties [46]. Further, it has been shown that the coordination linking of fluorescence organic ligands into a coordination network emits fluorescence emissions at an enhanced intensity, and this is ascribed to the long-range electronic communications between the adjacent ligands [45]. Herein, we combined the fluorescence Tröger's base linker **TBNap** with Zn(II) ion to gener-

ate the nanoscale coordination polymer **TB-Zn-CP** and explored its fluorescence-sensing properties towards various antibiotics in a water medium. **TB-Zn-CP** was taken in Milli-Q water and sonicated to obtain a well-dispersed aqueous colloidal suspension, which was subsequently used for fluorescence sensing studies. The UV-visible absorption of **TB-Zn-CP** displayed the typical spectrum of a high-energy band at $\lambda = 352$ nm, corresponding to the π-π^* transition, and a low-energy absorption band at $\lambda = 419$ nm due to the internal charge transfer (ICT) transition (Figure S5, Supplementary Materials). The fluorescence emission spectrum of **TB-Zn-CP** showed a broad emission band centered at $\lambda = 599$ nm due to the "push–pull"-based ICT transition (Figure S6, Supplementary Materials).
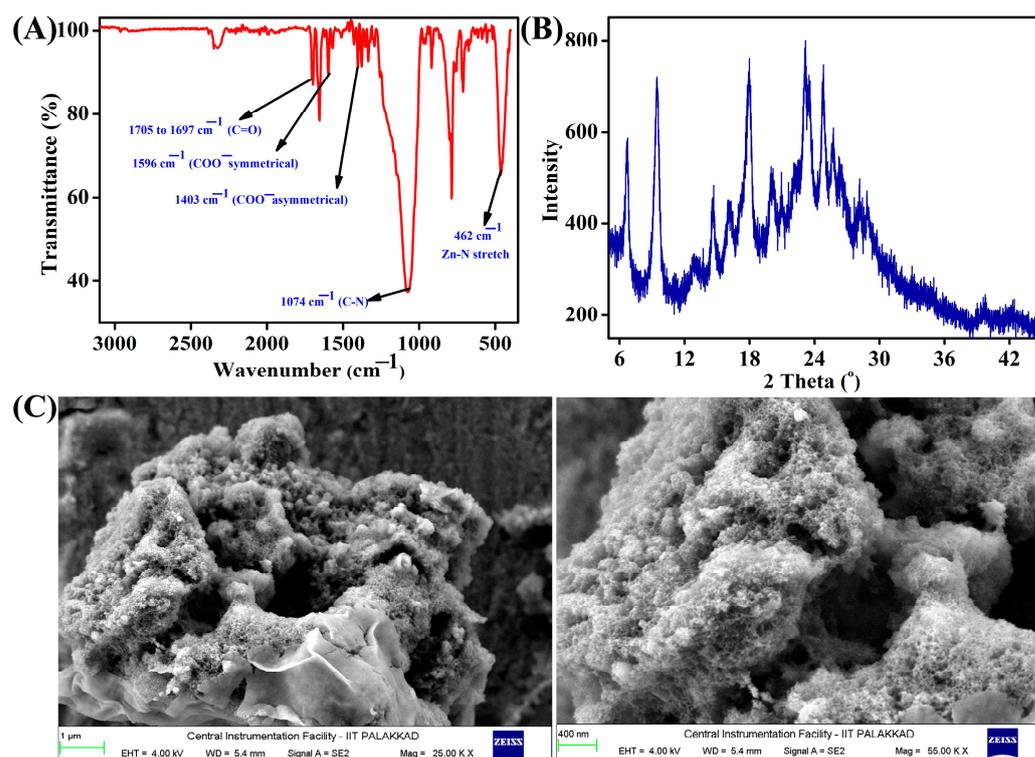

Figure 1. (**A**) The FTIR spectrum, (**B**) powder X-ray diffraction pattern, and (**C**) SEM images at different magnifications for **TB-Zn-CP**.

Inspired by the strong fluorescence emission, we next assessed the fluorescence-sensing property of **TB-Zn-CP** towards various antibiotics in water mediums. We chose different environmentally hazardous antibiotics, including Nitrofurantoin (NFT), Nitro-furazone (NFZ), Chloramphenicol (CRP), Furazolidone (FZD), Sulfadiazine (SDZ), 1,2-Dimethyl-5-nitroimidazole (DMZ), and Sulfamethazine (SMZ). First, a 1 mM stock solution of antibiotics was freshly prepared in Milli-Q water. To corroborate the selectivity of **TB-Zn-CP** in terms of sensing different antibiotics, we first measured the fluorescence emission intensity of **TB-Zn-CP** before and after the addition of various antibiotics. As depicted in Figure 2A,B, the coordination polymer **TB-Zn-CP** exhibited differential fluorescence-quenching responses for different antibiotics. Among the tested antibiotics, the DMZ, SMZ, and CRP antibiotics showed the largest fluorescence-quenching efficiency, while other antibiotics, NFT, NFZ, FZD, and SDZ, displayed moderate to poor fluorescence-quenching effects. The observed differential fluorescence-quenching responses for various antibiotics were also seen by sharp visual color changes (Figure 2C). Notably, the addition of SMZ and DMZ antibiotics changed the color of **TB-Zn-CP** from a bright greenish-yellow to colorless, but the mixing of other tested antibiotics showed no observable color changes.
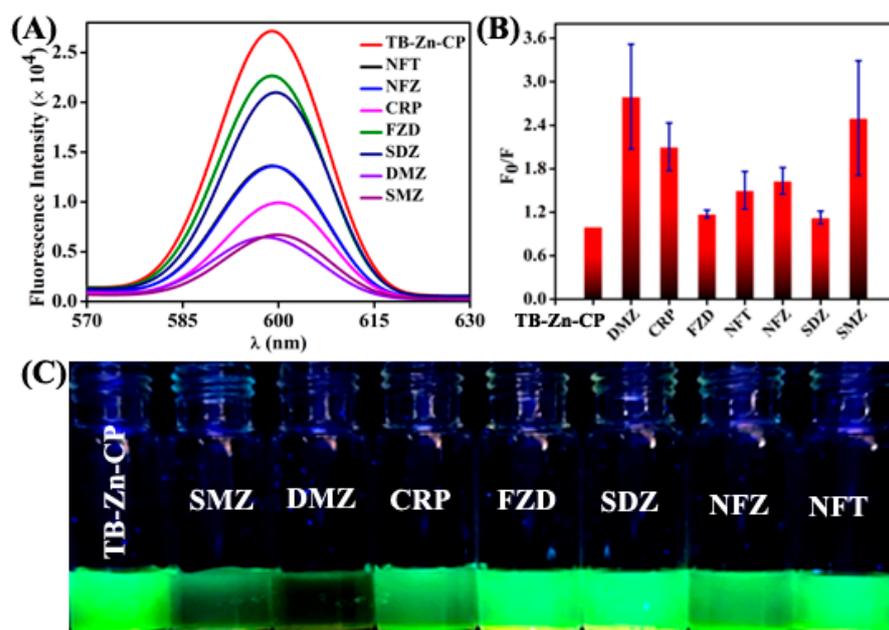
Figure 2. (**A**) The fluorescence emission spectra of **TB-Zn-CP** in the presence of different antibiotics and (**B**) corresponding bar diagram with error bar. (**C**) Observed visual color changes for **TB-Zn-CP** in the presence of antibiotics in water, imaged under UV light irradiation (Nitrofurantoin, NFT; Nitrofurazone, NFZ; Chloramphenicol, CRP; Furazolidone, FZD; Sulfadiazine, SDZ; 1,2-Dimethyl-5-nitroimidazole, DMZ; and Sulfamethazine, SMZ).

We next performed fluorescence titration studies to probe the binding between **TB-Zn-CP** and the antibiotics DMZ, SMZ, and CRP in an aqueous medium. The initial fluorescence emission intensity of **TB-Zn-CP** was gradually decreased with the gradual increases in the concentrations (0.0 to 99.9 μM) of antibiotics (Figure 3A), and the quenching efficiency was found to be 60% for DMZ, 53% for SMZ, and 50% for CRP, indicating the strong interactions between sensor **TB-Zn-CP** and antibiotics. Except for the attenuation of fluorescence emission intensity, no other spectral changes, such as a shift in the emission maxima or the appearance of any peaks, were observed. In all cases, a linear Stern–Volmer plot was obtained, and the Stern–Volmer quenching constant (K_{SV}) was determined to be 2.86×10^4 M^{-1} for DMZ, 2.61×10^4 M^{-1} for SMZ, and 2.85×10^4 M^{-1} for CRP (Figure 3B). The calculated K_{SV} values for different antibiotics from the fluorescence titration are summarized in Table 1. These values are comparable to those reported for other luminescence coordination polymer-based fluorescence sensors for antibiotics detection [60,61]. The high binding constant and sensing in a water medium make **TB-Zn-CP** a practically useful fluorescence sensor system for antibiotics detection.

To further investigate the binding between **TB-Zn-CP** and antibiotics, a UV–visible absorption titration study was performed using DMZ as representative antibiotics. Upon the addition of DMZ from 0.0 to 90.9 μM, the peak at λ = 419 nm decreased in its intensity, which was accompanied by an increase in intensity at λ = 317 nm and also a clear isosbestic point at λ = 387 nm, indicating the equilibrium ground state charge transfer (CT) complexation between **TB-Zn-CP** and DMZ (Figure 4A) [62]. A linear Stern–Volmer plot, significant changes in the absorption spectrum, and sharp visual color changes for **TB-Zn-CP** with the addition of DMZ antibiotic demonstrate that the observed fluorescence-quenching follows a static quenching mechanism via the formation of a ground-state non-fluorescent charge transfer complex between **TB-Zn-CP** and the antibiotics. The observed highest fluorescence-quenching for DMZ antibiotics, compared with the others, is presumably due to its more electron-deficient nature, caused by the electron-withdrawing -NO$_2$ group. To check the sensitivity of **TB-Zn-CP**, further fluorescence titration studies were performed by taking the antibiotics DMZ, SMZ, and CRP at nanomolar (nM) concentrations. Interestingly,

it was found that **TB-Zn-CP** can sense antibiotics at the nM level of concentrations. The limit of detection (LoD) values for DMZ, SMZ, and CRP were determined to be 9.3 nM, 12.9 nM, and 25.5 nM, respectively. This level of sensitivity is much lower than that reported for several other fluorescence sensors and within the allowed concentration level [60].
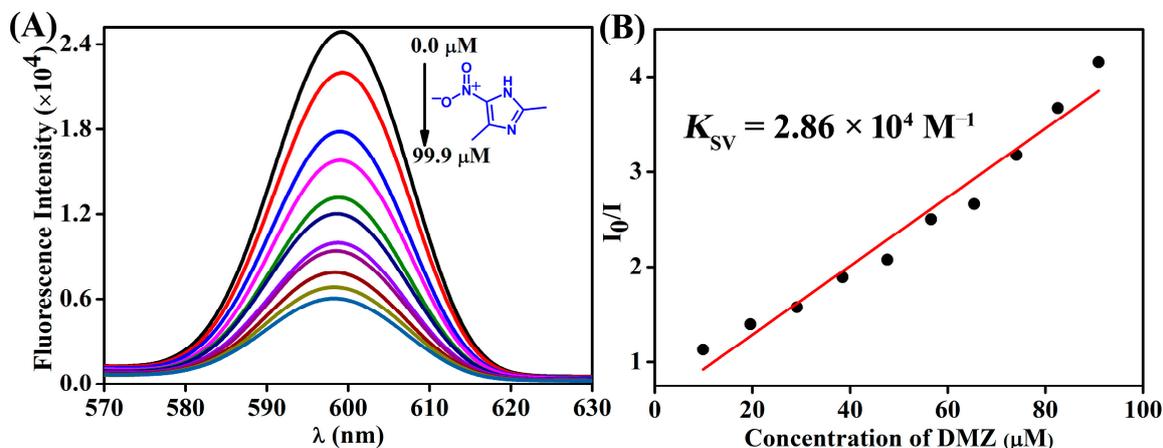

Figure 3. (**A**) The observed fluorescence emission-quenching of **TB-Zn-CP** with the gradual addition of 5-nitroimidazole (DMZ) antibiotic in water and (**B**) its corresponding Stern–Volmer plot.

Table 1. The calculated Stern–Volmer quenching constant (K_{SV}) for different antibiotics.

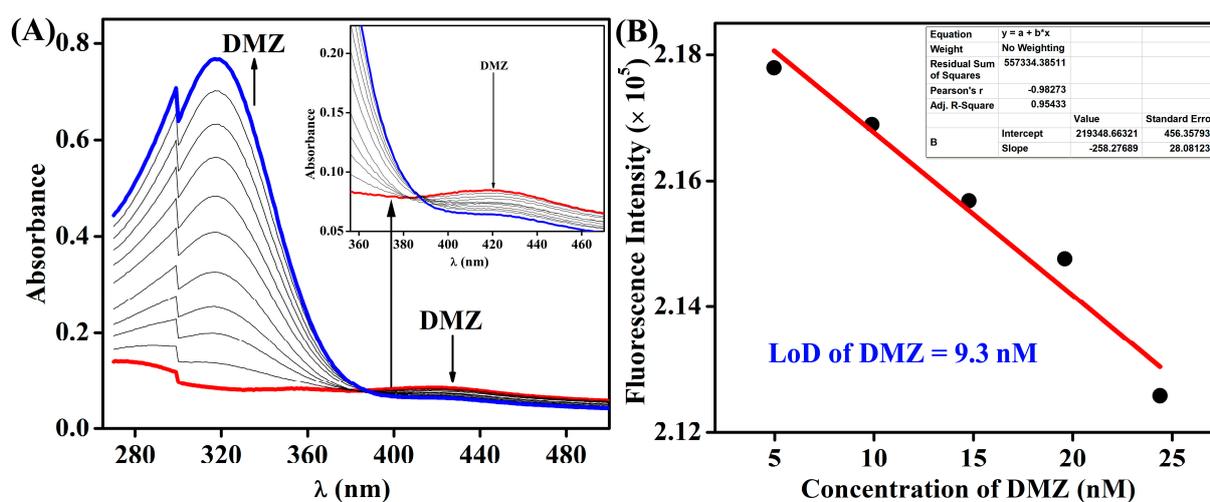| Antibiotics	K_{SV} ($\times 10^4$ M^{-1})
DMZ	2.86
SMZ	2.61
CRP	2.85
NFT	0.58
NFZ	0.14
SDZ	0.57
FZD	0.42

Figure 4. (**A**) The changes in the UV–visible absorption spectrum of **TB-Zn-CP** dispersed in water with the incremental addition of DMZ (from 0.0 to 90.9 μM). (**B**) The sensitivity plot of changes in emission intensity of **TB-Zn-CP** upon increasing the concentration of 5-nitroimidazole (DMZ) at the nM level.

4. Conclusions

In summary, we have developed a new nitrogen-rich luminescent Zn(II) coordination polymer, **TB-Zn-CP,** based on 4-amino-1,8-naphthalimide Tröger's base (**TBNap**) structural motif for differential fluorescence sensing of antibiotics in water mediums. The characterization using various spectroscopy and microscopy techniques indicated that **TB-Zn-CP** is a microcrystalline powder with sponge-like morphological features and exhibits high thermal stability. Owing to the strong ICT-based fluorescence emission, **TB-Zn-CP** was employed as a potential fluorescence chemosensor for antibiotic detection. **TB-Zn-CP** demonstrated differential fluorescence-sensing properties for different antibiotics, with high quenching efficiency and preferred sensing ability for antibiotics such as SMZ, DMZ, and CRP. The differential sensing ability of **TB-Zn-CP** was also seen by marked color changes, and fluorescence titration studies also conveyed that **TB-Zn-CP** can sense antibiotics at a nanomolar level of concentrations. In conclusion, all the studies discussed herein demonstrate that **TB-Zn-CP** can be a potential and practically useful fluorescence and visual sensor for the differential, quick, and ultra-sensitive sensing of antibiotic contaminants in water. Further work is in progress to design highly porous coordination polymer-based **TBNap** scaffolds and explore their applications as molecular adsorbents for the efficient adsorption and removal of emerging and persistent organic contaminants in water.

Supplementary Materials: The following supporting information can be downloaded at: https://www.mdpi.com/article/10.3390/chemistry6010011/s1, Figure S1: The FTIR spectrum of ligand TBNap; Figure S2: The particle size distribution data was obtained by DLS measurement for the polymer TB-Zn-CP in an aqueous medium; Figure S3: Thermogravimetric analysis (TGA) spectrum of TB-Zn-CP; Figure S4: (A) Energy dispersive X-ray spectroscopy (EDX) data and (B) Quanta mapping images for TB-Zn-CP; Figure S5: UV-visible absorption spectrum of TB-Zn-CP measured in water; Figure S6: The fluorescence emission spectrum of TB-Zn-CP was recorded in water.

Author Contributions: Investigation, M.K.N. and P.P.; writing—original draft preparation, M.K.N., P.P. and S.S.; writing—review and editing, M.K.N. and S.S.; supervision, S.S.; project administration, S.S.; funding acquisition, S.S. All authors have read and agreed to the published version of the manuscript.

Data Availability Statement: The raw data supporting the conclusions of this article will be made available by the authors on request.

Conflicts of Interest: The authors declare no conflicts of interest.

References

1. Mesak, L.R.; Miao, V.; Davies, J. Effects of Subinhibitory Concentrations of Antibiotics on SOS and DNA Repair Gene Expression in *Staphylococcus aureus*. *Antimicrob. Agents Chemother.* **2008**, *52*, 3394–3397. [CrossRef]
2. Yi, H.; Huang, D.; Qin, L.; Zeng, G.; Lai, C.; Cheng, M.; Ye, S.; Song, B.; Ren, X.; Guo, X. Selective Prepared Carbon Nanomaterials for Advanced Photocatalytic Application in Environmental Pollutant Treatment and Hydrogen Production. *Appl. Catal. B Environ.* **2018**, *239*, 408–424. [CrossRef]
3. Paul, M.; Shani, V.; Muchtar, E.; Kariv, G.; Robenshtok, E.; Leibovici, L. Systematic Review and Meta-Analysis of the Efficacy of Appropriate Empiric Antibiotic Therapy for Sepsis. *Antimicrob. Agents Chemother.* **2010**, *54*, 4851–4863. [CrossRef]
4. Huang, D.; Wang, X.; Zhang, C.; Zeng, G.; Peng, Z.; Zhou, J.; Cheng, M.; Wang, R.; Hu, Z.; Qin, X. Sorptive Removal of Ionizable Antibiotic Sulfamethazine from Aqueous Solution by Graphene Oxide-Coated Biochar Nanocomposites: Influencing Factors and Mechanism. *Chemosphere* **2017**, *186*, 414–421. [CrossRef]
5. Davies, J. What Are Antibiotics? Archaic Functions for Modern Activities. *Mol. Microbiol.* **1990**, *4*, 1227–1232. [CrossRef]

6. Zhang, C.; Lai, C.; Zeng, G.; Huang, D.; Yang, C.; Wang, Y.; Zhou, Y.; Cheng, M. Efficacy of Carbonaceous Nanocomposites for Sorbing Ionizable Antibiotic Sulfamethazine from Aqueous Solution. *Water Res.* **2016**, *95*, 103–112. [CrossRef]

7. Klein, E.Y.; Van Boeckel, T.P.; Martinez, E.M.; Pant, S.; Gandra, S.; Levin, S.A.; Goossens, H.; Laxminarayan, R. Global Increase and Geographic Convergence in Antibiotic Consumption between 2000 and 2015. *Proc. Natl. Acad. Sci. USA* **2018**, *115*, E3463–E3470. [CrossRef]

8. Morrison, L.; Zembower, T.R. Antimicrobial Resistance. *Gastrointest. Endosc. Clin.* **2020**, *30*, 619–635. [CrossRef]

9. Zhao, D.; Liu, X.-H.; Zhao, Y.; Wang, P.; Liu, Y.; Azam, M.; Al-Resayes, S.I.; Lu, Y.; Sun, W.-Y. Luminescent Cd (II)–Organic Frameworks with Chelating NH 2 Sites for Selective Detection of Fe (III) and Antibiotics. *J. Mater. Chem. A* **2017**, *5*, 15797–15807. [CrossRef]

10. Zhu, X.-D.; Zhang, K.; Wang, Y.; Long, W.-W.; Sa, R.-J.; Liu, T.-F.; Lv, J. Fluorescent Metal–Organic Framework (MOF) as a Highly Sensitive and Quickly Responsive Chemical Sensor for the Detection of Antibiotics in Simulated Wastewater. *Inorg. Chem.* **2018**, *57*, 1060–1065. [CrossRef]

11. Xu, S.; Shi, J.-J.; Ding, B.; Liu, Z.-Y.; Wang, X.-G.; Zhao, X.-J.; Yang, E.-C. A Heterometallic Sodium (i)–Europium (iii)-Organic Layer Exhibiting Dual-Responsive Luminescent Sensing for Nitrofuran Antibiotics, $Cr_2O_7^{2-}$ and MnO_4^- Anions. *Dalton Trans.* **2019**, *48*, 1823–1834. [CrossRef]

12. Liu, X.-G.; Tao, C.-L.; Yu, H.-Q.; Chen, B.; Liu, Z.; Zhu, G.-P.; Zhao, Z.; Shen, L.; Tang, B.Z. A New Luminescent Metal–Organic Framework Based on Dicarboxyl-Substituted Tetraphenylethene for Efficient Detection of Nitro-Containing Explosives and Antibiotics in Aqueous Media. *J. Mater. Chem. C* **2018**, *6*, 2983–2988. [CrossRef]

13. Mungroo, N.A.; Neethirajan, S. Biosensors for the Detection of Antibiotics in Poultry Industry—A Review. *Biosensors* **2014**, *4*, 472–493. [CrossRef]

14. Li, Y.-T.; Qu, L.-L.; Li, D.-W.; Song, Q.-X.; Fathi, F.; Long, Y.-T. Rapid and Sensitive In-Situ Detection of Polar Antibiotics in Water Using a Disposable Ag–Graphene Sensor Based on Electrophoretic Preconcentration and Surface-Enhanced Raman Spectroscopy. *Biosens. Bioelectron.* **2013**, *43*, 94–100. [CrossRef]

15. Cinquina, A.L.; Longo, F.; Anastasi, G.; Giannetti, L.; Cozzani, R. Validation of a High-Performance Liquid Chromatography Method for the Determination of Oxytetracycline, Tetracycline, Chlortetracycline and Doxycycline in Bovine Milk and Muscle. *J. Chromatogr. A* **2003**, *987*, 227–233. [CrossRef]

16. Wickramanayake, P.U.; Tran, T.C.; Hughes, J.G.; Macka, M.; Simpson, N.; Marriott, P.J. Simultaneous Separation of Nitrofuran Antibiotics and Their Metabolites by Using Micellar Electrokinetic Capillary Chromatography. *Electrophoresis* **2006**, *27*, 4069–4077. [CrossRef]

17. Aguilera-Luiz, M.M.; Vidal, J.L.M.; Romero-Gonzalez, R.; Frenich, A.G. Multi-Residue Determination of Veterinary Drugs in Milk by Ultra-High-Pressure Liquid Chromatography–Tandem Mass Spectrometry. *J. Chromatogr. A* **2008**, *1205*, 10–16. [CrossRef]

18. Paul, T.; Miller, P.L.; Strathmann, T.J. Visible-Light-Mediated TiO_2 Photocatalysis of Fluoroquinolone Antibacterial Agents. *Environ. Sci. Technol.* **2007**, *41*, 4720–4727. [CrossRef]

19. González, O.; Sans, C.; Esplugas, S. Sulfamethoxazole Abatement by Photo-Fenton: Toxicity, Inhibition and Biodegradability Assessment of Intermediates. *J. Hazard. Mater.* **2007**, *146*, 459–464. [CrossRef]

20. Li, D.; Yang, M.; Hu, J.; Zhang, Y.; Chang, H.; Jin, F. Determination of Penicillin G and Its Degradation Products in a Penicillin Production Wastewater Treatment Plant and the Receiving River. *Water Res.* **2008**, *42*, 307–317. [CrossRef]

21. Germain, M.E.; Knapp, M.J. Optical Explosives Detection: From Color Changes to Fluorescence Turn-On. *Chem. Soc. Rev.* **2009**, *38*, 2543–2555. [CrossRef]

22. Ahmaruzzaman, M. Adsorption of Phenolic Compounds on Low-Cost Adsorbents: A Review. *Adv. Colloid Interface Sci.* **2008**, *143*, 48–67. [CrossRef]

23. Wanderley, M.M.; Wang, C.; Wu, C.-D.; Lin, W. A Chiral Porous Metal–Organic Framework for Highly Sensitive and Enantioselective Fluorescence Sensing of Amino Alcohols. *J. Am. Chem. Soc.* **2012**, *134*, 9050–9053. [CrossRef]

24. Nagarkar, S.S.; Desai, A.V.; Ghosh, S.K. A Fluorescent Metal–Organic Framework for Highly Selective Detection of Nitro Explosives in the Aqueous Phase. *Chem. Commun.* **2014**, *50*, 8915–8918. [CrossRef]

25. Lin, X.; Hong, Y.; Zhang, C.; Huang, R.; Wang, C.; Lin, W. Pre-Concentration and Energy Transfer Enable the Efficient Luminescence Sensing of Transition Metal Ions by Metal–Organic Frameworks. *Chem. Commun.* **2015**, *51*, 16996–16999. [CrossRef]

26. Cui, Y.; Yue, Y.; Qian, G.; Chen, B. Luminescent Functional Metal–Organic Frameworks. *Chem. Rev.* **2012**, *112*, 1126–1162. [CrossRef]

27. Kreno, L.E.; Leong, K.; Farha, O.K.; Allendorf, M.; Van Duyne, R.P.; Hupp, J.T. Metal–Organic Framework Materials as Chemical Sensors. *Chem. Rev.* **2012**, *112*, 1105–1125. [CrossRef]

28. Van de Voorde, B.; Bueken, B.; Denayer, J.; De Vos, D. Adsorptive Separation on Metal–Organic Frameworks in the Liquid Phase. *Chem. Soc. Rev.* **2014**, *43*, 5766–5788. [CrossRef]

29. Li, B.; Wen, H.-M.; Wang, H.; Wu, H.; Tyagi, M.; Yildirim, T.; Zhou, W.; Chen, B. A Porous Metal–Organic Framework with Dynamic Pyrimidine Groups Exhibiting Record High Methane Storage Working Capacity. *J. Am. Chem. Soc.* **2014**, *136*, 6207–6210. [CrossRef]

30. Wu, D.; Sedgwick, A.C.; Gunnlaugsson, T.; Akkaya, E.U.; Yoon, J.; James, T.D. Fluorescent Chemosensors: The Past, Present and Future. *Chem. Soc. Rev.* **2017**, *46*, 7105–7123. [CrossRef]

31. Shanmugaraju, S.; Mukherjee, P.S. π-Electron Rich Small Molecule Sensors for the Recognition of Nitroaromatics. *Chem. Commun.* **2015**, *51*, 16014–16032. [CrossRef]

32. Sun, X.; Wang, Y.; Lei, Y. Fluorescence Based Explosive Detection: From Mechanisms to Sensory Materials. *Chem. Soc. Rev.* **2015**, *44*, 8019–8061. [CrossRef]

33. Shanmugaraju, S.; Mukherjee, P.S. Self-assembled Discrete Molecules for Sensing Nitroaromatics. *Chem. Eur. J.* **2015**, *21*, 6656–6666. [CrossRef]

34. Erbas-Cakmak, S.; Kolemen, S.; Sedgwick, A.C.; Gunnlaugsson, T.; James, T.D.; Yoon, J.; Akkaya, E.U. Molecular Logic Gates: The Past, Present and Future. *Chem. Soc. Rev.* **2018**, *47*, 2228–2248. [CrossRef]

35. Suh, M.P.; Park, H.J.; Prasad, T.K.; Lim, D.-W. Hydrogen Storage in Metal–Organic Frameworks. *Chem. Rev.* **2012**, *112*, 782–835. [CrossRef]

36. Wang, B.; Lv, X.-L.; Feng, D.; Xie, L.-H.; Zhang, J.; Li, M.; Xie, Y.; Li, J.-R.; Zhou, H.-C. Highly Stable Zr (IV)-Based Metal–Organic Frameworks for the Detection and Removal of Antibiotics and Organic Explosives in Water. *J. Am. Chem. Soc.* **2016**, *138*, 6204–6216. [CrossRef]

37. Lustig, W.P.; Mukherjee, S.; Rudd, N.D.; Desai, A.V.; Li, J.; Ghosh, S.K. Metal–Organic Frameworks: Functional Luminescent and Photonic Materials for Sensing Applications. *Chem. Soc. Rev.* **2017**, *46*, 3242–3285. [CrossRef]

38. Chen, Z.; Jiang, H.; Li, M.; O'Keeffe, M.; Eddaoudi, M. Reticular Chemistry 3.2: Typical Minimal Edge-Transitive Derived and Related Nets for the Design and Synthesis of Metal–Organic Frameworks. *Chem. Rev.* **2020**, *120*, 8039–8065. [CrossRef]

39. Wu, S.; Zhu, M.; Zhang, Y.; Kosinova, M.; Fedin, V.P.; Gao, E. A Water-stable Lanthanide Coordination Polymer as Multicenter Platform for Ratiometric Luminescent Sensing Antibiotics. *Chem. Eur. J.* **2020**, *26*, 3137–3144. [CrossRef]

40. Liu, S.; Bai, J.; Huo, Y.; Ning, B.; Peng, Y.; Li, S.; Han, D.; Kang, W.; Gao, Z. A Zirconium-Porphyrin MOF-Based Ratiometric Fluorescent Biosensor for Rapid and Ultrasensitive Detection of Chloramphenicol. *Biosens. Bioelectron.* **2020**, *149*, 111801. [CrossRef]

41. Zhu, K.; Fan, R.; Zheng, X.; Wang, P.; Chen, W.; Sun, T.; Gai, S.; Zhou, X.; Yang, Y. Dual-Emitting Dye-CDs@ MOFs for Selective and Sensitive Identification of Antibiotics and MnO_4^- in Water. *J. Mater. Chem. C* **2019**, *7*, 15057–15065. [CrossRef]

42. Zhu, Q.-Q.; Zhou, Q.-S.; Zhang, H.-W.; Zhang, W.-W.; Lu, D.-Q.; Guo, M.-T.; Yuan, Y.; Sun, F.; He, H. Design and Construction of a Metal–Organic Framework as an Efficient Luminescent Sensor for Detecting Antibiotics. *Inorg. Chem.* **2020**, *59*, 1323–1331. [CrossRef]

43. Liu, Y.; Xie, X.-Y.; Cheng, C.; Shao, Z.-S.; Wang, H.-S. Strategies to Fabricate Metal–Organic Framework (MOF)-Based Luminescent Sensing Platforms. *J. Mater. Chem. C* **2019**, *7*, 10743–10763. [CrossRef]

44. Hawes, C.S.; Máille, G.M.Ó.; Byrne, K.; Schmitt, W.; Gunnlaugsson, T. Tetraarylpyrrolo[3,2-b]Pyrroles as Versatile and Responsive Fluorescent Linkers in Metal–Organic Frameworks. *Dalton Trans.* **2018**, *47*, 10080–10092. [CrossRef]

45. Shanmugaraju, S.; Dabadie, C.; Byrne, K.; Savyasachi, A.J.; Umadevi, D.; Schmitt, W.; Kitchen, J.A.; Gunnlaugsson, T. A Supramolecular Tröger's Base Derived Coordination Zinc Polymer for Fluorescent Sensing of Phenolic-Nitroaromatic Explosives in Water. *Chem. Sci.* **2017**, *8*, 1535–1546. [CrossRef]

46. Rudd, N.D.; Wang, H.; Fuentes-Fernandez, E.M.A.; Teat, S.J.; Chen, F.; Hall, G.; Chabal, Y.J.; Li, J. Highly Efficient Luminescent Metal–Organic Framework for the Simultaneous Detection and Removal of Heavy Metals from Water. *ACS Appl. Mater. Interfaces* **2016**, *8*, 30294–30303. [CrossRef]

47. Li, Y.; Liu, K.; Li, W.-J.; Guo, A.; Zhao, F.-Y.; Liu, H.; Ruan, W.-J. Coordination Polymer Nanoarchitecture for Nitroaromatic Sensing by Static Quenching Mechanism. *J. Phys. Chem. C* **2015**, *119*, 28544–28550. [CrossRef]

48. Desai, A.V.; Inamdar, A.I.; Ghosh, S.K.; Mukherjee, S.; Manna, B. Exploitation of Guest Accessible Aliphatic Amine Functionality of a Metal Organic Framework for Selective Detection of 2,4,6-Trinitrophenol (TNP) in Water. *Cryst. Growth Des.* **2015**, *15*, 4627–4634.

49. Joarder, B.; Desai, A.V.; Samanta, P.; Mukherjee, S.; Ghosh, S.K. Selective and Sensitive Aqueous-phase Detection of 2,4,6-trinitrophenol (TNP) by an Amine-functionalized Metal–Organic Framework. *Chem. Eur. J.* **2015**, *21*, 965–969. [CrossRef]

50. Ivy, M.A.; Gallagher, L.T.; Ellington, A.D.; Anslyn, E. V Exploration of Plasticizer and Plastic Explosive Detection and Differentiation with Serum Albumin Cross-Reactive Arrays. *Chem. Sci.* **2012**, *3*, 1773–1779. [CrossRef]

51. Song, B.-Q.; Qin, C.; Zhang, Y.-T.; Wu, X.-S.; Yang, L.; Shao, K.-Z.; Su, Z.-M. Spontaneous Chiral Resolution of a Rare 3D Self-Penetration Coordination Polymer for Sensitive Aqueous-Phase Detection of Picric Acid. *Dalton Trans.* **2015**, *44*, 18386–18394. [CrossRef]

52. Nagarkar, S.S.; Desai, A.V.; Samanta, P.; Ghosh, S.K. Aqueous Phase Selective Detection of 2,4,6-Trinitrophenol Using a Fluorescent Metal–Organic Framework with a Pendant Recognition Site. *Dalton Trans.* **2015**, *44*, 15175–15180. [CrossRef]

53. Banerjee, S.; Bright, S.A.; Smith, J.A.; Burgeat, J.; Martinez-Calvo, M.; Williams, D.C.; Kelly, J.M.; Gunnlaugsson, T. Supramolecular Approach to Enantioselective DNA Recognition Using Enantiomerically Resolved Cationic 4-Amino-1,8-naphthalimide-Based Tröger's Bases. *J. Org. Chem.* **2014**, *79*, 9272–9283. [CrossRef]

54. Veale, E.B.; Gunnlaugsson, T. Synthesis, Photophysical, and DNA Binding Studies of Fluorescent Troger's Base Derived 4-Amino-1,8-naphthalimide Supramolecular Clefts. *J. Org. Chem.* **2010**, *75*, 5513–5525. [CrossRef]

55. Murphy, S.; Bright, S.A.; Poynton, F.E.; McCabe, T.; Kitchen, J.A.; Veale, E.B.; Williams, D.C.; Gunnlaugsson, T. Synthesis, Photophysical and Cytotoxicity Evaluations of DNA Targeting Agents Based on 3-Amino-1,8-naphthalimide Derived Tröger's Bases. *Org. Biomol. Chem.* **2014**, *12*, 6610–6623. [CrossRef]

56. Banerjee, S.; Kitchen, J.A.; Bright, S.A.; O'Brien, J.E.; Williams, D.C.; Kelly, J.M.; Gunnlaugsson, T. Synthesis, Spectroscopic and Biological Studies of a Fluorescent Pt (II)(Terpy) Based 1,8-Naphthalimide Conjugate as a DNA Targeting Agent. *Chem. Commun.* **2013**, *49*, 8522–8524. [CrossRef]

57. Veale, E.B.; Frimannsson, D.O.; Lawler, M.; Gunnlaugsson, T. 4-Amino-1,8-Naphthalimide-Based Troger's Bases as High Affinity DNA Targeting Fluorescent Supramolecular Scaffolds. *Org. Lett.* **2009**, *11*, 4040–4043. [CrossRef]

58. Xu, Y.; Li, B.; Li, W.; Zhao, J.; Sun, S.; Pang, Y. "ICT-Not-Quenching" near Infrared Ratiometric Fluorescent Detection of Picric Acid in Aqueous Media. *Chem. Commun.* **2013**, *49*, 4764–4766. [CrossRef]

59. Lovitt, J.I.; Umadevi, D.; Raja Lakshmi, P.; Twamley, B.; Gunnlaugsson, T.; Shanmugaraju, S. Synthesis, Structural Characterization, Antibiotics Sensing and Coordination Chemistry of a Fluorescent 4-Amino-1,8-Naphthalimide Tröger's Base Supramolecular Scaffold. *Supramol. Chem.* **2020**, *32*, 620–633. [CrossRef]

60. Lakshmi, P.R.; Nanjan, P.; Kannan, S.; Shanmugaraju, S. Recent Advances in Luminescent Metal–Organic Frameworks (LMOFs) Based Fluorescent Sensors for Antibiotics. *Coord. Chem. Rev.* **2021**, *435*, 213793. [CrossRef]

61. Ghosh, S.; Rana, A.; Biswas, S. Metal–Organic Framework-Based Fluorescent Sensors for the Detection of Pharmaceutically Active Compounds. *Chem. Mater.* **2024**, *36*, 99–131. [CrossRef]

62. Shanmughan, A.; Lakshmi, P.R.; Umadevi, D.; Shanmugaraju, S. Discriminative Fluorescent Sensing of Nitro-Antibiotics at Ppb Level Using N-Phenyl-Amino-1,8-Naphthalimides Chemosensors. *Results Chem.* **2022**, *4*, 100546. [CrossRef]